Electronic differential for tramcar bogies: system development and performance evaluation by means of numerical simulation

Andrea N. Barbera, Giuseppe Bucca, Roberto Corradi, Alan Facchinetti* and Ferdinando Mapelli

Dipartimento di Meccanica, Politecnico di Milano, Via G. La Masa 1, I-20156 Milan, Italy

(*Received 12 November 2013; accepted 1 March 2014*)

1. Introduction

Wheelset configuration, with solid axle or independently rotating wheels (IRWs), has a remarkable effect on the dynamic performance of a tramcar vehicle.

Conventional solid axle wheelsets are characterised by a self-centring behaviour which allows to counteract the effects of lateral track irregularities, thus preventing or at least reducing the occurrences of flange contacts in tangent track. This self-centring behaviour is almost absent for IRWs, if the gravitational stiffness effect is neglected. As a consequence, bogies equipped with IRWs are very sensitive to track disturbances [1] and continuous flange contact may occur also in tangent track.[2]

Moreover, while during the negotiation of medium/large radius curves solid axle wheelsets provide steering and guidance capabilities [3] (in many cases even avoiding flange contact), in the case of sharp curved sections typical of urban networks IRWs experience much lower contact forces than solid axle wheelsets.[1,4] When negotiating such tight curves, as a consequence of the counter-steering torque associated with the opposite lateral creep forces acting

*Corresponding author. Email: alan.facchinetti@polimi.it

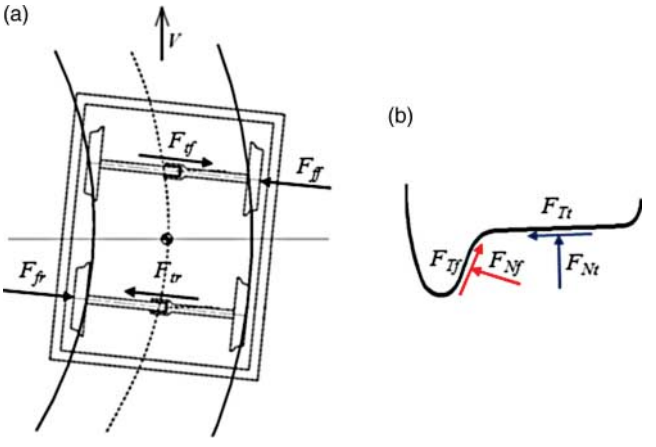

Figure 1. Tight curve negotiation of a tramcar bogie: (a) lateral forces on the treads of the front and rear axle (F_{tf} and F_{tr}) and lateral contact forces on the flange of the front outer and rear inner wheel (F_{ff} and F_{fr}) and (b) contact force distribution on the front outer wheel.

on the treads of the front and the rear axle (see F_{tf} and F_{tr} in Figure 1(a)), tramcar bogies are forced to run with both the front outer wheel and the rear inner wheel in the flange contact condition. In this situation, the lateral force F_{tf} on the flange of the front outer wheel, mainly resulting from the normal contact force F_{Nf} (Figure 1(b)), and the lateral force F_{tr} on the flange of the rear inner wheel, which presents a contact force distribution symmetric to the one reported in Figure 1(b), balance the counter-steering torque of the creep forces on the treads, thus keeping the bogie on the track.

In addition to this behaviour that is typical of any tramcar bogie, regardless of the wheelset configuration, significant longitudinal forces arise at the wheel–rail interface when considering solid axles, as a consequence of the wheelset-track relative lateral displacement (which results in opposite variations of the rolling radius on the two wheels), and of the different distance covered by the inner and the outer wheels.

During tight curve negotiation, the latter contribution prevails and leads to a counter-steering effect on the single wheelsets and on the overall bogie, resulting in a higher steady-state lateral contact force on the front outer wheel for a bogie equipped with solid wheelsets than for a running gear provided with IRWs.

The above-mentioned considerations lead one to conclude that it would be desirable to have a tramcar bogie behaving as if it were equipped with solid axles in tangent track and with IRWs in a curve.

This paper illustrates an electronic differential system to be applied to tramcar bogies equipped with wheel-hub motors, which allows switching from solid axles in tangent track to IRWs in sharp curve (and vice versa). The idea behind the proposed system is that of automatically activating/deactivating an electric shaft between the two wheels of an axle, according to a control logic based on the continuous monitoring of signals that are already available and can be easily collected from the electric drives (i.e. motor currents and angular speeds).

The electric shaft strategy can only be applied to bogies equipped with wheel-hub motors, so that each wheel can be driven separately and differential torques can be applied to the two wheels belonging to the same axle.

The paper is organised as follows: in Section 2, the motivations for the electronic differential are pointed out, considering some examples of the different behaviour of solid axles and IRWs in tangent track and in the tight curve. Section 3 describes the electro-mechanical model adopted for the simulation of the electronic differential, considering the mechanical model of

the vehicle and the electrical model of the wheel-hub motors. Section 4 defines the control strategy, which is based on hierarchical control layers. Finally, in Section 5 some significant results are discussed in order to evaluate the performances of the proposed system.

The reference vehicle considered in the paper is an urban-articulated tramcar (seven carbodies, four bogies and eight axles), with 35 m overall length and 57 kN mean axle load.

2. Solid axles vs. IRW: motivation for the electronic differential

As already mentioned, when running in a tangent track at a relatively low speed, solid axles show a better behaviour than IRWs, thanks to the capability of recovering the track central position if a lateral displacement occurs. This self-centring feature derives from the opposite longitudinal forces which act on the left and right wheels, as a consequence of the rolling radius variation which results from a lateral wheelset displacement. This effect is almost absent in IRWs, since wheel rotations are independent, and the only self-centring contribution may come from the gravitational stiffness.

With this respect, Figure 2 shows the time histories of the lateral forces acting on the four wheels of a bogie equipped with solid axles (Figure 2(a)) and of a bogie equipped with IRWs (Figure 2(b)). Lateral forces are assumed to be positive when pointing towards the left (the same sign convention is adopted in the rest of the paper). The results shown in Figure 2 refer to two numerical simulations carried out by means of the multibody software described in Section 3.1. In the two simulations, the same tramcar vehicle and the same running conditions are considered: tangent track section, vehicle speed of 40 km/h and track irregularity according to ERRI B176 standard (large amplitude defects).

When comparing Figure 2(a) and 2(b), it can be observed that the self-centring behaviour of solid axles allows avoiding, or at least limiting, the flange contact events with respect to the IRWs case, with a consequent reduction of the lateral force peaks, in terms of both amplitude and number of occurrences. The expected benefit is a lower wear rate, for both wheel and rail. Since wear rate is related to frictional power,[5,6] it is interesting to integrate the comparison between solid axles and IRWs, by computing the time histories of the power dissipated by the creep forces acting on the four wheels of the bogie (Figure 3), for the same two numerical simulations considered before. At each time step and for each wheel, the frictional power is computed on the basis of the creep forces and creep velocities in the different simultaneous contact patches. When looking at Figure 3, the better performance of the bogie with solid axles

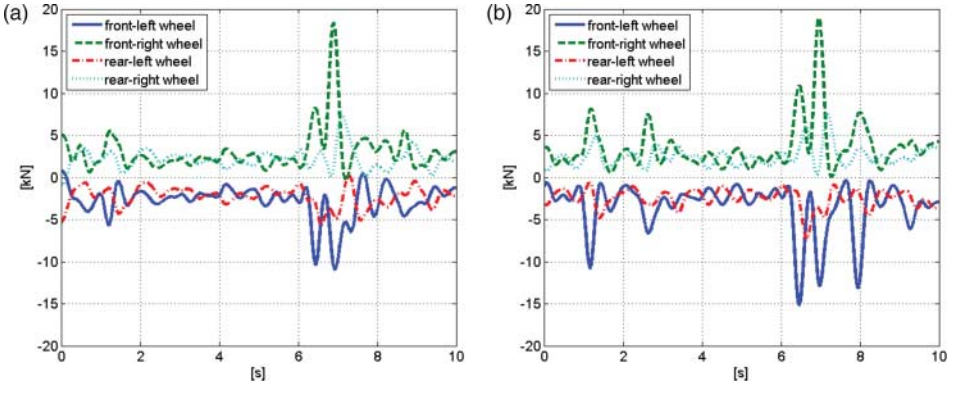

Figure 2. Wheel-rail lateral contact forces in tangent track – $V = 40$ km/h, track irregularity according to the ERRI B176 standard (large amplitude defects): (a) solid axles and (b) IRWs.

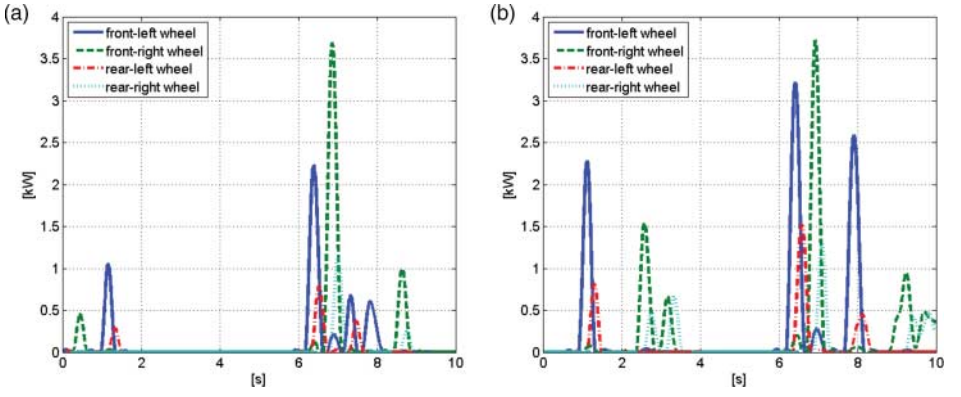

Figure 3. Frictional power in tangent track – $V = 40$ km/h, track irregularity according to the ERRI B176 standard (large amplitude defects): (a) solid axles and (b) IRWs.

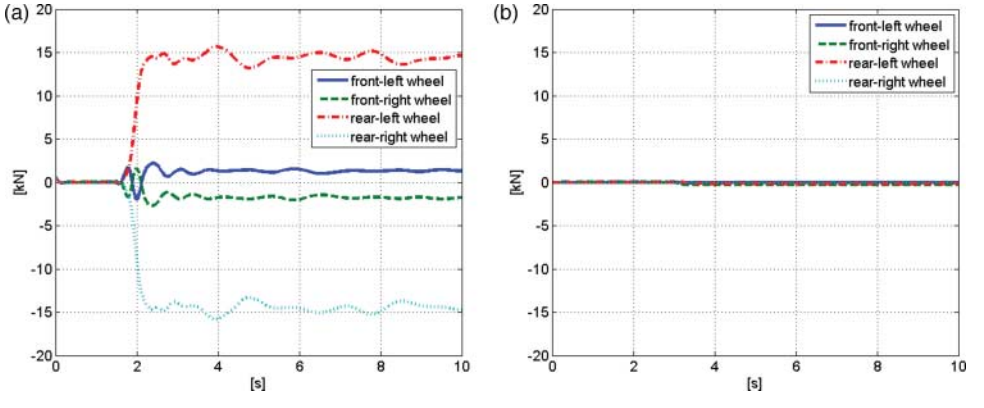

Figure 4. Wheel-rail longitudinal contact forces in curve – $V = 25$ km/h, $R = 100$ m: (a) solid axles and (b) IRWs.

is even more evident: the frictional power is significantly higher for the IRW configuration, the overall energy dissipated by friction being 5.7 kJ for the IRW bogie, against 3.7 kJ for the solid axle one, during the 10 s simulation in tangent track.

When sharp curve negotiation is analysed, opposite conclusions can be drawn. Relying again on the multibody software described in Section 3.1, the curving behaviour of solid axles and IRWs was investigated. In both cases, a traditional non-steering bogie (i.e. with parallel axles) is considered. Several numerical simulations were carried out, considering curves with different radii (in the range 25–300 m); in each simulation, the tramcar speed was adjusted so as to correspond to a fixed lateral acceleration (0.5 m/s^2). Based on the typical characteristics of many European tramway networks, in all the simulations no transition curve is considered.

Figure 4 shows the time histories of the wheel-rail longitudinal contact forces, in the case of solid axles and IRWs. In both cases, the tramcar vehicle is negotiating a 100 m radius left curve, at 25 km/h. IRWs show almost zero longitudinal forces (Figure 4(b)), whereas significant forces arise when considering the bogie equipped with solid axles (Figure 4(a)). Longitudinal forces are due to the presence of the solid axle, which imposes the angular speed of the two wheels to be equal, and are the result of two different mechanisms. First, the curvature radius of the inner rail is smaller than that of the outer one and, consequently, the inner wheel travels at a speed lower than that of the outer wheel. Second, whenever the wheelset is displaced from the centred position, the rolling radii on the two wheels become different. The two effects lead to opposite creepages and consequent opposite longitudinal

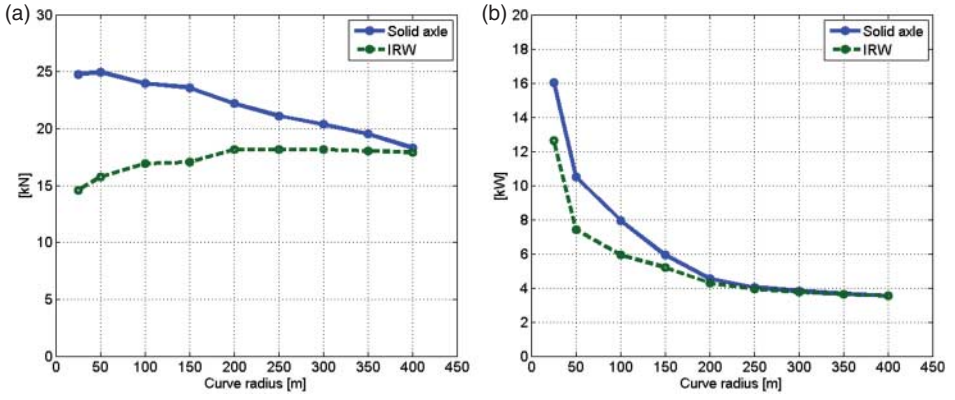

Figure 5. Steady-state curving behaviour as a function of the curve radius, for fixed lateral acceleration ($0.5\,m/s^2$): (a) lateral contact forces on the front outer wheel and (b) total frictional power on the bogie.

forces on the two wheels of an axle. During the negotiation of a sharp curve, such as the one under consideration, the first of the two effects mentioned above is predominant and a counter-steering yaw moment acts on the bogie, which produces an increase in the lateral contact force on the front outer wheel. The final outcome is a distribution of the lateral forces on the four wheels which is less balanced for a bogie with solid axles than for one with IRWs.

With this respect, Figure 5(a) compares the steady-state values of the lateral contact force on the front outer wheel, as a function of the curve radius, in the case of solid axles and IRWs. Figure 5(a) clearly shows that, during the negotiation of sharp curves (i.e. with radius lower than 350 m), a bogie equipped with solid axles experiences lateral forces on the front outer wheel which are much greater than those of a bogie with IRWs. Moreover, the steady-state frictional power (i.e. that being dissipated by the creep forces acting on all the bogie wheels, in full curve) is significantly higher in the case of solid axles, for curve radii lower than 200 m (Figure 5(b)).

According to the analyses illustrated above, it would be desirable to have a tramcar bogie behaving as if it were equipped with solid axles in tangent track and with IRWs in a curve.

This is the motivation for developing an electronic differential system to be applied to tramcar bogies, which allows switching from solid axles in tangent track to IRWs in a sharp curve (and vice versa). In order to implement such a control system, the running gear is provided with four wheel-hub motors, so that differential torques can be applied to the wheels belonging to the same axle.[7–9]

3. The electro-mechanical vehicle model

3.1. *The mechanical model*

The vehicle multibody model [10] allows the analysis of the non-stationary behaviour of a tramcar, running in tangent and curved tracks, with variable speed. Kinematic nonlinearities are fully accounted for.

In order to reproduce the most common configurations of modern tramcars, the numerical model has been designed to allow various combinations of two types of basic modules:

- module A, which is made up of one carbody and one bogie;
- module B, which is a single carbody, suspended between two type A modules.

The different modules can be linked to each other by means of kinematic constraints and/or elastic elements, reproducing the actual connections between the tramcar carbodies. Moreover, each module has parametric characteristics. In this way, various types of tramcars can be modelled.

The equations of motion of the complete vehicle are obtained applying Lagrange's equations and can be written in the following matrix form:

$$[M]\ddot{\underline{x}} + [C]\dot{\underline{x}} + [K]\underline{x} = \underline{Q}(\underline{x}, \dot{\underline{x}}, t), \tag{1}$$

where

- $\underline{x}$ is the vector containing the independent coordinates of the whole mechanical model;
- $[M]$, $[C]$ and $[K]$ are the mass, damping and stiffness matrices of the entire tramcar;
- vector $\underline{Q}$ contains the generalised forces associated with:
  - the connections between carbodies;
  - the nonlinear terms associated with vehicle's inertia;
  - the nonlinear wheel–rail contact forces;
  - the effect of the bumpstops;
  - the track irregularity excitation;
  - the driving/braking torques on the wheels.

The numerical model adopted to compute the wheel-rail contact forces [11] is designed for reproducing the actual contact conditions specific of tramways, even in the case of grooved rail, worn wheel/rail profiles and in the presence of multiple contact patches. The solution of the contact problem, i.e. the calculation of the normal contact forces and of the transversal and longitudinal creep forces, is split into three sequential steps: first, a preliminary geometrical analysis is performed once for all before the numerical simulation, then for each wheel and at each time step the normal contact problem is solved, and finally creep forces are computed.

In order to solve the normal contact problem, a multi-hertzian model is adopted. Once the normal contact problem is solved, the creep forces acting in the tangential plane are evaluated. The longitudinal and transversal creepages on each contact area can be easily determined, since the wheelset kinematics at the generic integration step is known. Then, the transversal and longitudinal creep forces are determined through the Shen–Hedrick–Elkins heuristic formulation. Also track irregularity excitation can be accounted for, by means of imposed vertical and lateral displacements, applied to the rail profile.

Reference is made to [10] for a detailed description of the numerical procedure that has been implemented to calculate the vehicle mass, stiffness and damping matrices, and the vector $\underline{Q}$ of the generalised forces.

The vehicle mechanical model described above was extensively validated by means of comparison with experimental data collected during on-track test campaigns.[12]

3.2. *The electrical model*

In order to model the dynamic behaviour of the permanent magnet synchronous motors which generate the driving/braking torques applied to each wheel-hub motor, Equations (2) are adopted. These equations are based on the space vector theory, which allows to switch from the phase variables (voltages v_a, v_b, v_c and currents i_a, i_b, i_c) to the corresponding quantities in the (d, q) coordinate system, i.e. a coordinate system synchronous with the permanent magnet

flux:

$$
\begin{aligned}
v_{\mathrm{sd}} &= R_{\mathrm{s}} i_{\mathrm{sd}} - \dot{\vartheta} L_{\mathrm{s}} i_{\mathrm{sq}} + L_{\mathrm{s}} \frac{\mathrm{d}i_{\mathrm{sd}}}{\mathrm{d}t}, \\
v_{\mathrm{sq}} &= R_{\mathrm{s}} i_{\mathrm{sq}} + \dot{\vartheta} \psi_{\mathrm{m}} + \dot{\vartheta} L_{\mathrm{s}} i_{\mathrm{sd}} + L_{\mathrm{s}} \frac{\mathrm{d}i_{\mathrm{sq}}}{\mathrm{d}t}, \\
T_{\mathrm{m}} - T_{\mathrm{r}} &= J_{\mathrm{mot}} \ddot{\vartheta}_{\mathrm{w}}, \\
T_{\mathrm{m}} &= n \psi_{\mathrm{m}} i_{\mathrm{sq}}.
\end{aligned}
\tag{2}
$$

In Equations (2), v_{sd} and i_{sd} represent the stator voltage phasor and the current phasor components, with respect to the direct axis (the coordinate axis directed as the permanent magnet flux), v_{sq} and i_{sq} represent the stator voltage phasor and the current phasor components corresponding to the quadrature axis (the coordinate axis oriented at 90° with respect to the permanent magnet flux), R_{s} and L_{s} are the equivalent stator resistance and inductance, ψ_{m} is the permanent magnet flux, $\dot{\vartheta}$ is the electrical angular velocity, related to the wheel angular velocity $\dot{\vartheta}_{\mathrm{w}}$ through the pole pairs number n ($\dot{\vartheta} = n\,\dot{\vartheta}_{\mathrm{w}}$), T_{m}, T_{r} and J_{mot} are, respectively, the electromagnetic torque, the resisting torque and the rotor's moment of inertia.

This formulation emphasises that it is possible to adjust the quadrature (q) current component, which is directly related to the electromagnetic torque value, by acting on the stator quadrature voltage component. In this way, it is possible to control the driving/braking torque to the wheel.

The electrical equations (2), written for each wheel-hub motor, are added to the mechanical equations (1) and coupled with them through the relationship between the electrical angular velocity and the wheel angular speed ($\dot{\vartheta} = n\,\dot{\vartheta}_{\mathrm{w}}$). The complete set of equations is rearranged in terms of a state-space model, in which the state variables are the mechanical independent coordinates $\underline{x}$, their time derivatives $\underline{\dot{x}}$, and the electrical currents i_{sd}, i_{sq} of each wheel-hub motor in the (d, q) coordinate system. The system state equations are updated at each time step and numerically integrated in the time domain.

4. The control system

The simulation software includes not only the electro-mechanical model of the tramcar vehicle and of the electric motors, but it also accounts for the control system, which acts at three different hierarchical levels:

- EDCS (Electronic Differential Control System), higher layer;
- ESCS (Electric Shaft Control System), intermediate layer;
- DCS (Drive Control System), lower layer.

The EDCS is responsible for the automatic activation/deactivation of the electric shaft, depending on whether the bogie is running in tangent track or in a curve. In the former case, the reference torque to the two wheel-hub motors of a certain axle is provided by the ESCS, while in the latter case the two reference torques are the same (i.e. zero in coasting, or a driver-defined value in case of traction/braking). Since many European tramway networks implement curves with no transition, this is the reference condition considered in the paper. Therefore, the activation/deactivation of the electric shaft is assumed to be instantaneous.

The ESCS is the feedback control system which is responsible for making the two wheels of a certain axle rotate at the same angular speed. When being activated by the EDCS, the ESCS provides proper reference torques to the two wheel-hub motors, so that the two wheels

behave as if they were connected by a rigid shaft, resulting in equal rotating speeds. For this reason this kind of control is commonly referred to as the electric shaft control. It is important to point out that the reference torques provided by the ESCS represent equal and opposite deltas, which sum up with the driver-defined torque. In other words, the mean value of the reference torques to the two wheel-hub motors is zero in the case of coasting, while it is equal to the driver-defined value in the case of traction/braking.

The DCS is the drive control system of a single wheel-hub motor. The DCS implements the vector control algorithm for a permanent magnet synchronous motor. The DCS receives the reference torque directly from the EDCS (when the bogie is running in curve) or through the ESCS (when the bogie is running in tangent track) and provides the proper phase input voltages as input to the motor.

In the next paragraphs, the three hierarchical control systems will be presented. The lower layer (DCS) will be described first, followed by the intermediate (ESCS) and higher (EDCS) ones.

4.1. *Drive Control System*

The DCS is responsible for controlling the phase input voltages to the permanent magnet synchronous motor, so as to follow the reference torque.

The DCS can be described starting from the block diagram of Figure 6. The vector control acts on the voltage space vector components referred to the rotating reference frame d, q. This makes possible to obtain a sort of equivalent DC motor control. The current space vector components $i_{\mathrm{sd}}, i_{\mathrm{sq}}$ can be calculated by means of measuring the three phase currents i_{a}, i_{b} and i_{c} and the Park transformation matrix $T(\theta)$. The voltages that have to be applied to the motor ($v_{a,b,c}$) can be obtained from the voltages $v_{\mathrm{d,q}}$ calculated by the DC motor equivalent control, through the reverse Park transformation $T^{-1}(\theta)$.

In the block diagram of Figure 6, it is possible to identify the block that calculates the PWM pulses (GS PWM) and the power inverter that supplies the motor with the desired three phase voltages. The regulator block consists of two PI controllers, one for each current component.

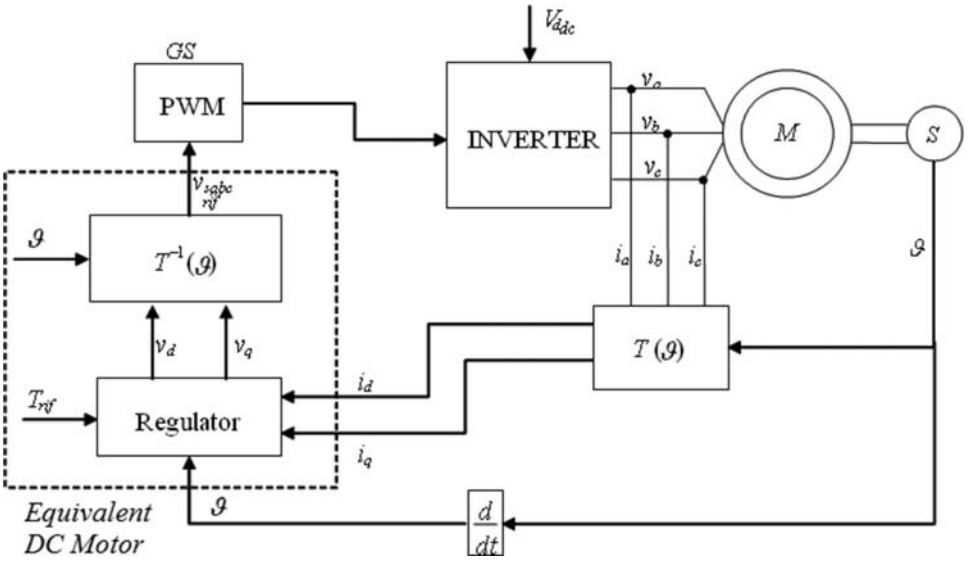

Figure 6. Block diagram of the vector-controlled permanent magnet synchronous motor.

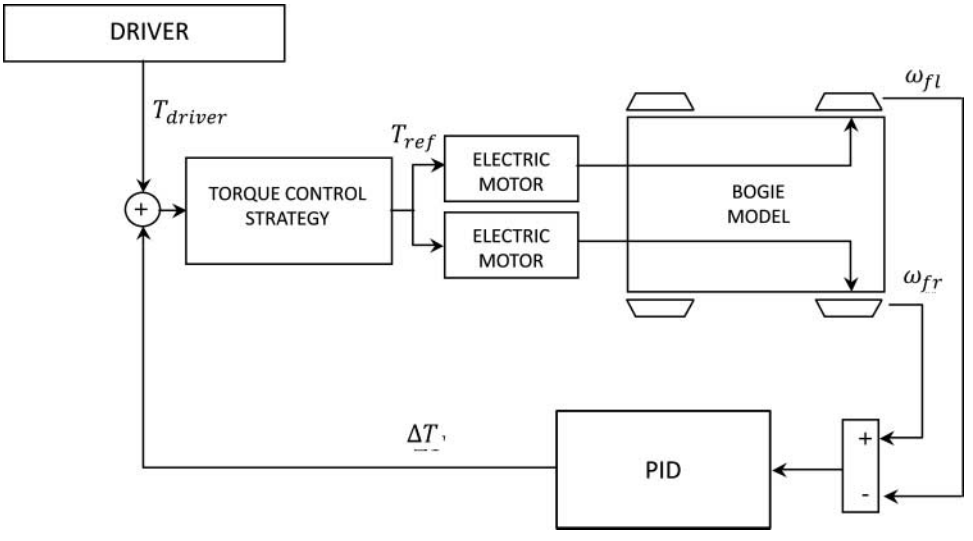

Figure 7. Block diagram of the ESCS.

Actually, the i_{sd} component is set to zero, since no field weakening is considered for this application.

The DCS model implemented into the vehicle simulator has been simplified in that the power inverter and the PWM blocks are assumed to be ideal, their time response being very fast with respect to the other elements of the electro-mechanical system. In this way, the blocks $T(\theta)$ and $T(\theta)^{-1}$ are directly coupled and result into an equivalent unit block.

The DCS of each wheel-hub motor has been provided with saturated output and reference, in order to account for the real torque limits of the traction drives. A per unit scaling is also adopted for the current controllers.

4.2. *Electric Shaft Control System*

In Section 2, the reason for preferring solid axle architecture when running in tangent track has been shown. By means of the ESCS, also when dealing with a bogie equipped with IRWs, it is possible to reproduce the dynamic behaviour of solid axles. The ESCS (see Figure 7) receives as input the measured angular speeds of the wheels belonging to the same axle (e.g. ω_{fl} and ω_{fr}) and computes the difference between them. This difference is then fed into a PID regulator which provides as output the delta torque ΔT which is added to/subtracted from the driver-defined torque, to obtain the references for the two wheel-hub motors. In this way the control system introduces an electric shaft between the two wheels, which simulates the presence of a solid axle connecting them.

Tangent track simulations performed by means of the electro-mechanical vehicle simulator described in Section 3, with activated ESCS, demonstrated that this control system is fully capable of reproducing the self-centring behaviour typical of a solid axle: results almost identical to those of Figures 2(a) and 3(a) were obtained.

4.3. *Electronic differential control system*

The EDCS is based on a threshold control logic, which means that the activation/deactivation of the electric shaft depends on the crossing of properly tuned thresholds. When entering a

curve, the EDCS provides automatic deactivation of the electric shaft, which is activated again when the bogie exits from the curve and enters a tangent track section.

The choice of which parameters need to be monitored in order to identify curve entrance/exit, together with the definition of the threshold values to be adopted, was the basis for the EDCS design. In order to develop the most effective control strategy, several numerical simulations were carried out by means of the electro-mechanical vehicle model described in Section 3. Two different conditions were considered: curve entrance with the electric shaft activated and curve exit with the electric shaft deactivated. The results of these simulations are presented in the two following sections.

4.3.1. *Curve entrance analysis*

The purpose of this set of numerical simulations is to choose the variables to be monitored for the identification of curve entrance and to tune the corresponding thresholds for the deactivation of the electric shaft. In fact, since the bogie is getting out from a tangent track section, in all numerical simulations the ESCS is supposed to be active.

A fixed curve radius of 100 m and a running speed of 25 km/h are considered, while the following parameters are varied:

- axle loads (tare or full load);
- track irregularity (no irregularity or track irregularity according to ERRI standard);
- driver-defined torque.

Figure 8 shows the reference torques required by the ESCS and the time histories of the wheel angular speeds, for the simulation in tare condition, wit the vehicle in coasting and no track irregularity.

As soon as the bogie enters the curve, a sudden increase in the reference torques occurs. This increase is particularly evident on the trailing axle, since the longitudinal forces on this axle are definitely higher than those on the leading one (see the typical behaviour in a curve of a bogie equipped with solid axles, Section 2).

With reference to Figure 8, it is worth remarking that the DCS of each wheel-hub motor has been provided with saturated output and reference, in order to account for the real torque limits of the traction drives. This is the reason for the saturation of the torque reference signals

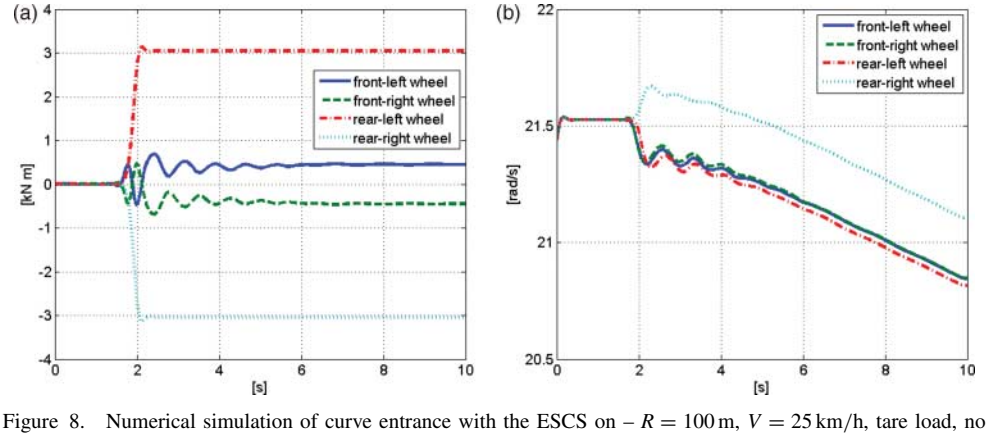

Figure 8. Numerical simulation of curve entrance with the ESCS on – $R = 100$ m, $V = 25$ km/h, tare load, no track irregularity: (a) time histories of the reference torques required by the ESCS and (b) time histories of the wheel angular speeds.

on the rear axle (Figure 8(a)), and the consequent difference in the two wheel angular speeds (Figure 8(b)).

Based on the results shown in Figure 8(a), it is clear that the difference between the reference torques required by the ESCS on the trailing axle can be usefully adopted as the quantity to be monitored for the deactivation of the electric shaft.

The performed sensitivity analysis (the results of which are not reported here for the sake of conciseness) showed that the difference between the reference torques is smaller for the tare load configuration, which therefore represents the most critical condition for tuning the threshold value. On the other hand, the presence of track irregularity showed a negligible effect on the torque difference, whereas the introduction of a driver-defined torque further reduced the difference.

Additional simulations were performed for the definition of the most suitable threshold, so as to investigate the effects of curve radius (from 25 to 200 m) and of lateral acceleration (0.5 and 0.8 m/s^2).

According to the results obtained, the most critical situation is that of a very sharp curve ($R = 25$ m), in the presence of a driver-defined braking torque (corresponding to a deceleration of 0.9 m/s^2). Based on this result, 4000 Nm was set as the threshold value for the difference of the reference torques required by the ESCS: if the latter quantity on the trailing axle overcomes the specified threshold for more than 0.5 s, thus indicating the entrance in a curved section, the electric shaft is automatically deactivated. Note that the threshold value indicated above is much higher than the torque difference required by the ESCS, in the case of running on a tangent track section with certain irregularity.

4.3.2. *Curve exit analysis*

Once the vehicle is running in full curve, with the ESCS off, a new problem needs to be faced, which consists in identifying when the bogie reaches the end of the curve, so as to activate again the electric shaft.

Figure 9 shows the time histories of the wheel angular speeds and of the difference between the angular speeds of the wheels belonging to the same axle, when the tramcar is running on a left curve with 100 m radius at 25 km/h, with the ESCS off. The simulation refers to tare load condition, with the vehicle in coasting and no track irregularity. The considered bogie enters the curve at approximately 2 s and exits from it at 9 s.

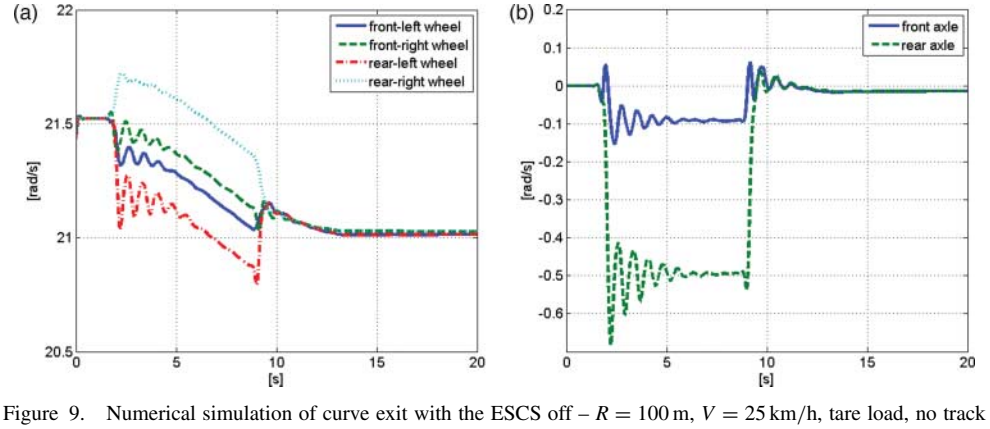

Figure 9. Numerical simulation of curve exit with the ESCS off – $R = 100$ m, $V = 25$ km/h, tare load, no track irregularity: (a) time histories of the wheel angular speeds and (b) time histories of the differences between the angular speeds of the wheels belonging to the same axle.

Since the ESCS is off, the wheels are independently rotating. In full curve, the difference between the wheel angular speeds on the trailing axle is larger than the same quantity computed on the leading axle. As soon as the bogie gets out of the curve, the wheel angular speeds become equal. Therefore, the angular speeds of the two trailing wheels are chosen as the signals to be monitored for the detection of the exit from a curved section: when the difference between them decreases under a certain threshold value, the electric shaft is activated again.

In order to properly tune the threshold value, a sensitivity analysis has been performed, in which the influence of the curve radius (from 25 to 200 m) and of the driver-defined torque is investigated. The results of this sensitivity analysis allowed setting the threshold value at 0.05 rad/s. Moreover, with the aim of reducing the effect of track irregularity, which leads to random oscillations in the angular speed signals, the monitored signals are low-pass filtered by means of a moving average procedure.

5. Results

Once that the EDCS logic for the activation/deactivation of the electric shaft has been established by means of the analysis reported in Section 4.3, it is implemented in the simulation software for the analysis of tramcar dynamics, in order to verify its effectiveness and its robustness.

As discussed before, the control strategy is based on the continuous monitoring of the torques on the trailing axle wheels, which is needed to maintain the electric shaft active: when the difference between the reference torques overcomes for a time interval of 0.5 s the threshold value (4000 Nm), the electric shaft is deactivated in 0.1 s, thus switching to IRWs. Once the electric shaft is deactivated, it is the difference of the angular speed of the rear axle wheels which is being monitored, and its moving average (over a time interval of 2 s) is compared with the threshold value, fixed to 0.05 rad/s: when this moving average value gets lower than the imposed threshold, the tramcar vehicle is assumed to be running in tangent track, and the electric shaft is activated again.

In order to verify the performances of the electronic differential, a sample simulation is analysed considering a track section composed of a short tangent track, a 50 m long curved track with a radius of 100 m, and a final tangent track. The running speed is 36 km/h and track irregularity is taken into account, according to ERRI B176, large amplitude defects.

Figure 10 shows the time histories of the torques applied to the wheels of the first bogie (Figure 10(a)) and of the difference between the angular speeds, for the front and rear axle wheels (Figure 10(b)). Analysing this figure, it is possible to verify the correct operation of the EDCS. In particular, it can be observed that when the reference torque on the rear axle wheels increases and overcomes the threshold value (at $t = 1.4$ s approximately), the control deactivates the electric shaft and the vehicle negotiates the whole curve behaving as a vehicle with IRWs. At the end of the curved section ($t = 6.7$ s), the difference of the trailing wheel angular speed steeply decreases under the threshold value and the electric shaft is reactivated ($t = 8.3$ s)). In this condition, the torque applied to the wheels guarantees the self-centring behaviour of the bogie axles.

Figure 11(a) shows the lateral contact forces on the four wheels of the first bogie. The same quantities are reported in Figure 11(b) and 11(c) for the solid axle and the IRW configuration, respectively, in order to compare them with the proposed electronic differential. As it is possible to notice, the EDCS produces the expected performances: during curve negotiation the dynamic behaviour is equal to the one produced by the IRWs except for the very beginning of the curve, due to the deactivation time of the electric shaft. The guidance force on the front

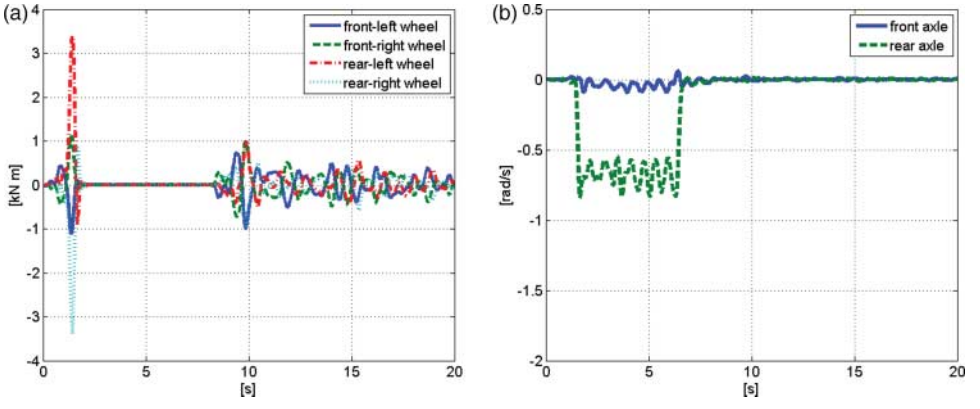

Figure 10. Bogie with electronic differential (tare load condition, constant speed, $V = 36\,\mathrm{km/h}$, track irregularity according to ERRI standard): time histories of (a) the torques applied to the wheels and (b) the difference between the angular speeds of the wheels belonging to the same axle.

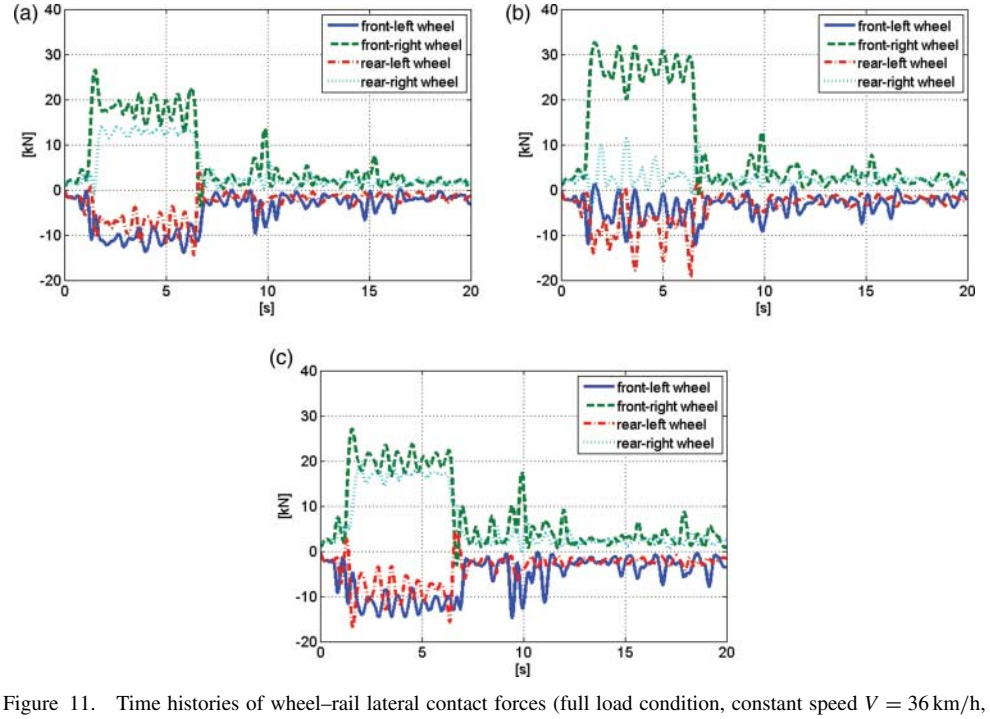

Figure 11. Time histories of wheel–rail lateral contact forces (full load condition, constant speed $V = 36\,\mathrm{km/h}$, track irregularity according to the ERRI standard): (a) bogie with electronic differential, (b) solid axles and (c) IRWs.

outer wheel is significantly lower than that observed for the solid axle configuration, along the entire curve.

After curve exit (at 6.5 s approximately) the reactivation of the electric shaft allows to obtain a behaviour very similar to that observed for solid axles. In particular, the number of flange contact occurrences and the values of the corresponding peaks in the lateral forces are significantly lower than those experienced by the simple IRW configuration.

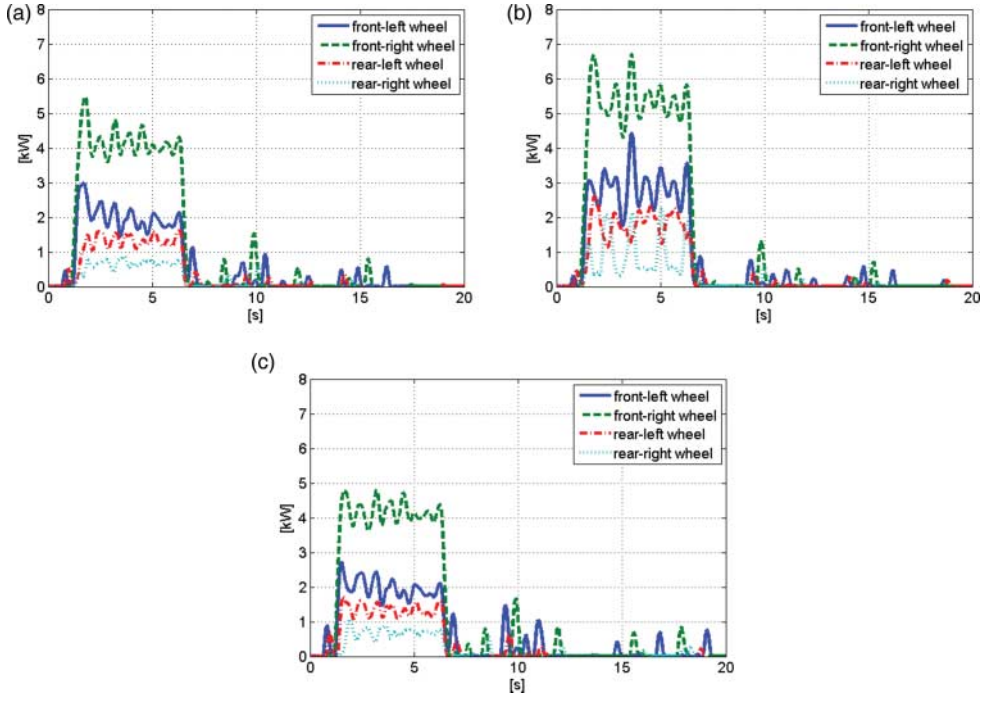

Figure 12. Time histories of the frictional power (full load condition, constant speed $V = 36$ km/h, track irregularity according to ERRI standard): (a) bogie with electronic differential, (b) solid axles and (c) IRWs.

The good performances of the electronic differential are even more evident when analysing the frictional power on the four wheels of the bogie (Figure 12). During curve negotiation, the frictional power with the electronic differential (Figure 12(a)) is the same observed with the IRW configuration (Figure 12(c)) and significantly lower than that obtained with solid axles (Figure 12(b)) for all the wheels. On the other hand, similarly to solid axles, in the following tangent track section the frictional power is reduced in comparison with that observed for IRWs. The final result is that the energy dissipated by friction in the overall simulation is 45.3 kJ for the bogie with electronic differential, 59.0 kJ for the solid axles and 46.0 kJ for IRWs. The small reduction of the dissipated energy achieved by the introduction of the electronic differential with respect to the simple IRW configuration is due on one side to the small incidence of the energy dissipated in tangent track, with respect to that dissipated in curve and, on the other side, to the higher frictional power at curve entrance observed with the electronic differential, which is related to the deactivation time of the electric shaft.

In order to verify the system behaviour in the presence of a driver-defined torque, a numerical simulation is considered, with the same track section and initial vehicle speed. A braking torque is applied while the first bogie is entering the curve, then it is released and, when the vehicle has completely left the curve, a traction torque is finally imposed.

Figure 13 shows the time histories of the torques applied to the wheels of the first bogie (Figure 13(a)) and the difference between the angular speeds of the front and rear axle wheels (Figure 13(b)). As it can be observed, also in this case the deactivation of the electric shaft at curve entrance ($t = 1.4$ s) and the reactivation in tangent track after curve exit ($t = 7.9$ s) take place properly, regardless of the applied driver-defined torques (braking from 1 to 4.8 s and traction from 10.8 to 14.6 s).

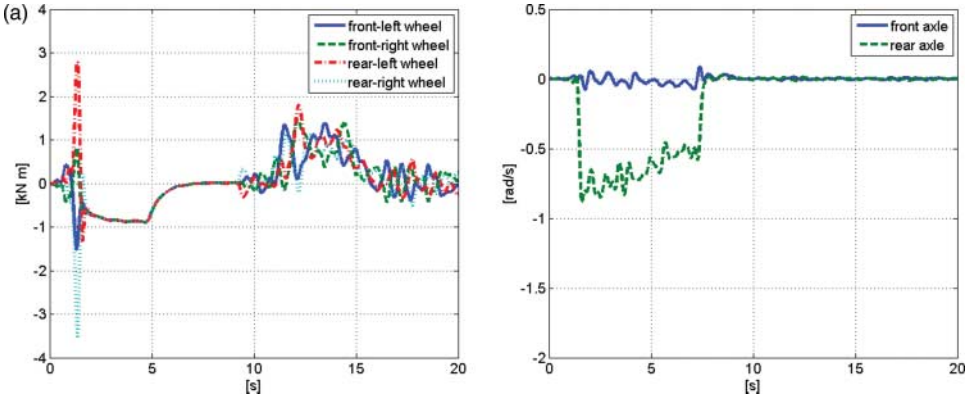

Figure 13. Bogie with electronic differential (the tare load condition, braking torque at curve entrance and traction torque at curve exit, average speed $V = 36$ km/h, track irregularity according to the ERRI standard): time histories of (a) the torques applied to the wheels and (b) the difference between the angular speeds of the wheels belonging to the same axle.

6. Conclusions

An electronic differential system to be applied to tramcar bogies with independently driven wheels has been proposed, which allows conjugating the benefits of solid axles in tangent track and of IRWs in a curve.

The system has been designed with the support of numerical simulations performed with a software developed by the authors, implementing an electro-mechanical model which includes a vehicle multibody model and an electrical model of the wheel-hub motors. The control system is based on hierarchical layers which are fully integrated in the simulation software.

The proposed electronic differential system does not require any structural modification to the bogie, provided that the bogie itself be equipped with IRWs and that the wheels be independently driven, e.g. through wheel-hub motors. The basic idea is that of automatically activating/deactivating an electric shaft between the two wheels of an axle, according to a control logic based on the continuous monitoring of signals that are already available and can be easily collected from the electric drives (i.e. motor currents and angular speeds).

At present, the activation/deactivation of the electric shaft is assumed to be instantaneous, since reference is made to curves with no transition, which are typical of many European tramway networks. In the presence of transition curves, the proposed control system could be easily upgraded to allow a smooth shift from electric shaft onto electric shaft off and vice versa.

The results illustrated in the paper demonstrate the effectiveness of the electronic differential system in improving the vehicle dynamic performances, in terms of force distribution in curve and of frictional power reduction in both tangent track and curve.

References

[1] Kuba T, Lugner P. Dynamic behaviour of tramways with different kinds of bogies. Veh Syst Dyn. 2012;50(S1):277–289. doi:10.1080/00423114.2012.666356

[2] Sugiyama H, Matsumura R, Suda Y, Ezaki H. Dynamics of independently rotating wheel system in the analysis of multibody railroad vehicles. J Comput Nonlinear Dyn. 2011;6(1):art. no. 011007. doi:10.1115/1.4002089

[3] Boocock D. Steady-state motion of railway vehicles on curved track. J Mech Eng Sci. 1969;11(6):556–566.

[4] Corradi R, Diana G, Facchinetti A. Sharp curve negotiation analysis of tramcar vehicles with different bogie architectures. Proceedings of the First International Conference on railway technology: research, development and maintenance; 2012; Stirlingshire (UK):Civil-Comp Press. Paper 129. doi:10.4203/ccp.98.129

[5] Beretta S, Braghin F, Bucca G, Desimone H. Structural integrity analysis of a tram-way: load spectra and material damage. Wear. 2005;258:1255–1264.
[6] Franklin FJ, Chung T, Kapoor A. Ratcheting and fatigue-led wear in rail-wheel contact. Fatigue Fract Eng Mater Struct. 2003;26:949–955.
[7] Mei TX, Goodall RM. Robust control for independently rotating wheelsets on a railway vehicle using practical sensors. IEEE Trans Control Syst Technol. 2001;9(4):599–607. doi:10.1109/87.930970
[8] Pérez J, Busturia JM, Mei TX, Viñolas J. Combined active steering and traction for mechatronic bogie vehicles with independently rotating wheels. Ann Rev Control. 2004;28(2):207–217. doi:10.1016/j.arcontrol.2004.02.004
[9] Feng J, Li J, Goodall RM. Integrated control strategies for railway vehicles with independently-driven wheel motors. Front Mech Eng China. 2008;3(3):239–250.
[10] Belforte P, Cheli F, Corradi R, Facchinetti A. Software for the Numerical Simulation of Tramcar Vehicle Dynamics. Heavy Veh Syst. 2003;19(1–2):48–69. doi:10.1504/IJHVS.2003.002434
[11] Cheli F, Corradi R, Diana G, Facchinetti A. Wheel-rail contact phenomena and derailment conditions in light urban vehicles. 6th international conference on contact mechanics and wear of rail/wheel systems (CM2003); 2003 June 10–13; Goteborg, Sweden.
[12] Cheli F, Corradi R, Diana G, Facchinetti A. Validation of a numerical model for the simulation of tramcar vehicle dynamics by means of comparison with experimental data. J Comput Nonlinear Dyn. 2007;2(4):299–309. doi:10.1115/1.2754306